
Electronic Supplementary Information for

In Situ Manipulation of Fluorescence Resonance Energy Transfer between Quantum Dots and Monolayer Graphene Oxide by Laser Irradiation

Wenjun He, Chengbing Qin*, Zhixing Qiao, Yani Gong, Xiaorong Zhang, Guofeng Zhang, Ruiyun Chen, Yan Gao, Liantuan Xiao*, and Suotang Jia

State Key Laboratory of Quantum Optics and Quantum Optics Devices, Institute of Laser Spectroscopy, Shanxi University, Taiyuan, 030006, China

Collaborative Innovation Center of Extreme Optics, Shanxi University, Taiyuan, Shanxi, 030006, China

Contents

1. AFM and SEM characterizations of PMMA film

To illustrate the preparation of PMMA film and characterize the structure of prepared sample, we provide the AFM and SEM characterizations of PMMA film with different thickness, as shown in Figure S1. Here, the PMMA with thickness about 5 nm, 15 nm, 34 nm, and 3 μm were prepared with the following parameters:

- ❐ 5 nm: the concentration of PMMA is 0.01 wt%, the spin-coating parameters are 500 rmp for 5s, 3000 rmp for 60 s, and 600 rmp for 10 s in turns;
- ❐ 15 nm: the concentration of PMMA is 0.1 wt%, the spin-coating parameters are 500 rmp for 5s, 3000 rmp for 60 s, and 600 rmp for 10 s in turns;
- ❐ 34 nm: the concentration of PMMA is 0.1 wt%, the spin-coating parameters are 500 rmp for 5s, 1000 rmp for 60 s, and 600 rmp for 10 s in turns;
- ❐ 3 μm: the concentration of PMMA is 1 wt%, and drop down PMMA to glass directly.

On should emphasized that the slight variation in the thickness of PMMA film may be occurred when operating by these parameters.

Comparing with the bare glass (Figure S1a), the presence of PMMA film can be clearly observed from the cross-sections shown in Figure S1b, as the white film with some aggregated balls on the top of glass substrate (the crack-like patterns on the cross-section of glass substrate results from the sputter coating of gold). By changing the concentration of PMMA solution and the operating parameters of spin-coating process, the thickness of extremely thick PMMA film can be clearly determined, as shown in Figure S1c. However, unfortunately, the layer-by-layer structure of GO/PMMA/QDs used in our experiment cannot be clearly observed, as shown in Figure S1d, 1g, and 1j, respectively. This limitation results from the resolution of our SEM apparatus (SU8010, Hitachi, Japan) and the extremely thin structure, where the thickness of GO and QDs are about 1.5 nm and 5 nm, and that of PMMA is in the region of 5-50 nm. Consequently, the thickness of them are still characterized by AFM, as shown in Figure S1e-1l, respectively.

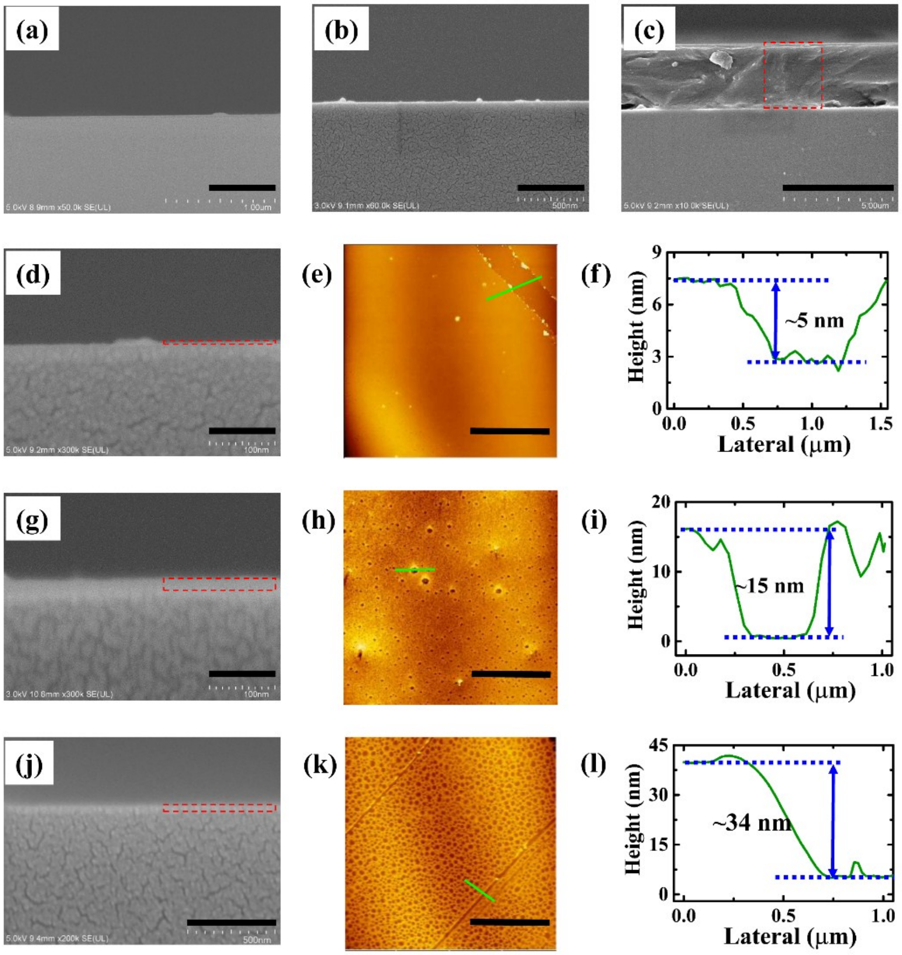

Figure S1. Cross-sectional SEM and AFM images of PMMA film with different thickness. The presence of PMMA has been highlighted by dashed rectangles. Cross-sectional SEM images of (a) bare glass, PMMA film with thickness of (b) 15 nm and (c) ~3.0 μm. (d-f) Cross-sectional SEM image, AFM image and height profile of PMMA with thickness about 5 nm. (g-i) Cross-sectional SEM image, AFM image and height profile of PMMA with thickness about 15 nm. (j-l) Cross-sectional SEM image, AFM image and height profile of PMMA with thickness about 34 nm. Scale bars (a) 1 μm; (b) 500 nm; (c) 5 μm; (d) 100nm; (e) 2 μm; (g) 100 nm; (h) 2 μm; (j) 500 nm; and (k) 2 μm.

2. TEM and AFM characterizations of QDs.

The near infrared emitting CdSeTe/ZnS core-shell QDs (Qdot®800 ITK^{TM} Organic QDs) were ordered from Thermo Fisher Scientific. The transmission electron microscope (TEM) image of QDs is shown in Figure S2a. It can be found that the CdSeTe/ZnS QDs have different shapes, from equilateral triangle to isosceles triangle, even circles. The size distribution of CdSeTe/ZnS QDs has been presented in Figure S2b. The size of the QDs distributes from 3.6 nm to 9.6 nm, with average diameter of ~ 6.4 nm. The wide distribution hints the strong anisotropic properties of QDs, as its lifetime distribution shown in Figure 4a. Figure S2c and S2d also present the AFM characterization of QDs and the height profile of the selected line. The average height of the QDs is about 5 nm.

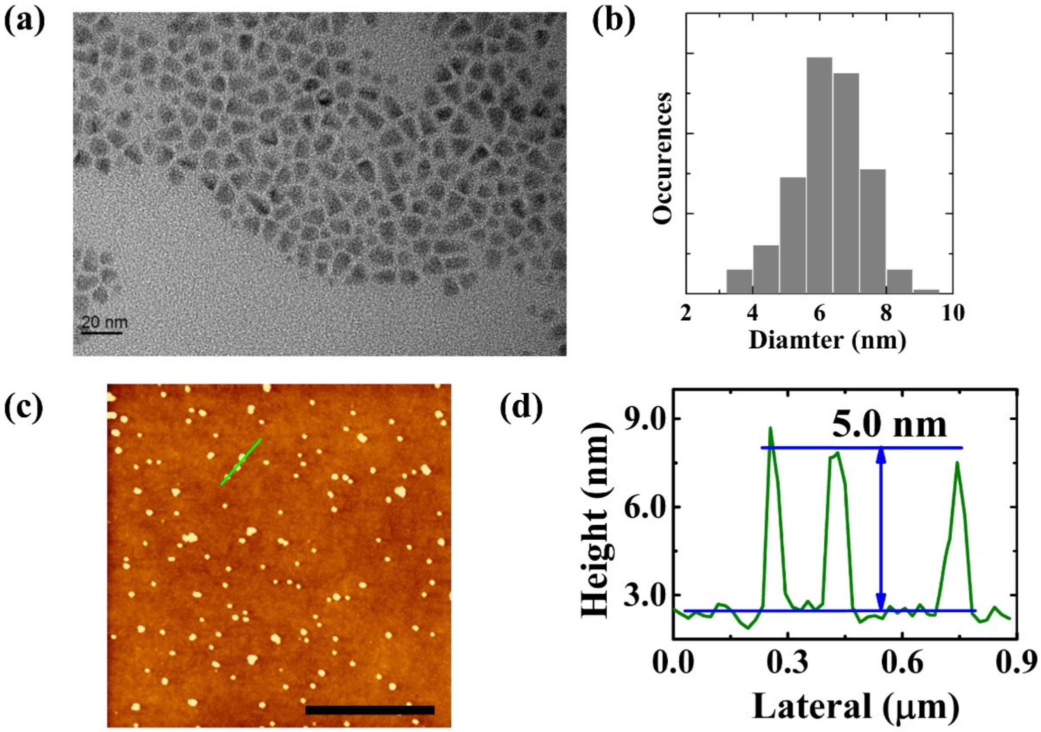

Figure S2. (a) TEM image of CdSeTe/ZnS QDs. (b) Statistical analysis on TEM image yielding the size distribution. (c) AFM characterization of CdSeTe/ZnS QDs and (d) the height profile of selected line. Scale bar: 2 μm.

3. Raman spectra of monolayer GO and reduced GO.

Raman spectra was used to confirm that the large flake in fluorescence imaging (Figure 1d) is originating from GO. Here Raman spectra was recorded using a custom-built Raman system equipped with a 532 nm laser source and a long focus monochromator (Horbia Jobin Yvon, 1250M). Figure S3 presents the Raman spectra taking from the area of large flake, as the circle shown in Figure S3a. Two main peaks can be clearly determined in the Raman spectra at 1335 and 1585 cm^{-1}, respectively. The two peaks can be assigned to *D* and *G* bands of GO, corresponding to ordered sp^2-bonded carbon and disordered sp^3 bonds in the C-C bonds, respectively. Thus, the large flakes can be undoubtedly attributed to the fluorescence emission of GO. Figure S3b further presents the Raman spectra of GO after irradiated with control laser with duration of 180 s. The increased intensity ratio of the *D* to *G* band (I_D/I_G) indicates the presence of smaller but more numerous sp^2 fragments and the removal of oxygen-containing functional groups. This phenomenon strongly suggests the photoreduction of GO after laser irradiation.

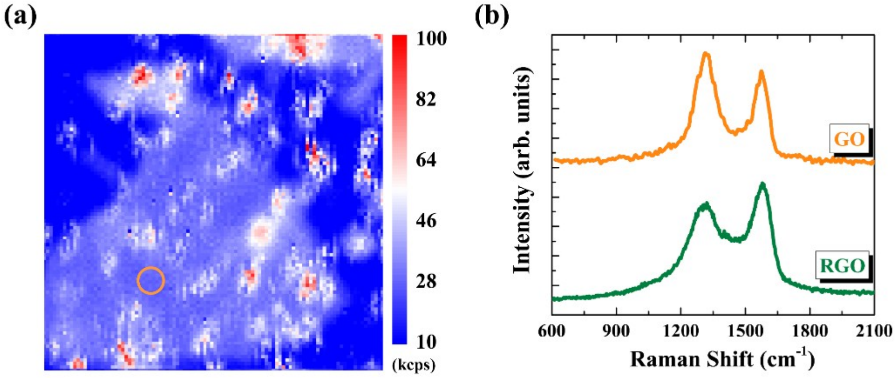

Figure S3. (a) Fluorescence intensity imaging of QDs-GO hybrid structure. The area highlighted by circle is used to take Raman spectra. (b) Raman spectra of GO and RGO with irradiation duration of 180 s.

4. The determination of single QD in the experiment

Generally, the determination of single QD is firstly guaranteed by the sample preparation. During sample preparation, the concentration of QDs and the operating parameters of spin-coating process are carefully optimized to obtain well-dispersed QDs on the substrates. The morphology of prepared sample is then checked by AFM, as shown in Figure S4. Even though some aggregated QDs still can be found (highlighted by green circles), most of them are individual particle.

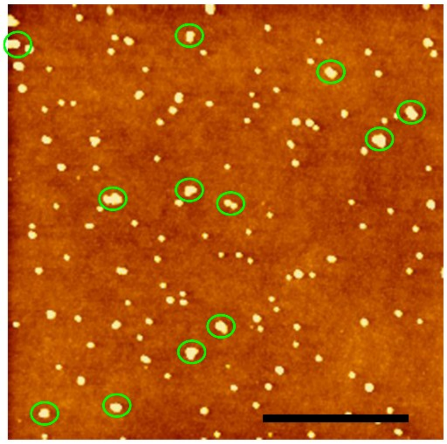

Figure S4. AFM characterization of prepared QDs. The QDs highlighted by green circles might be aggregated QDs. Scale bar: 2 μm.

Then, the single QD will be further checked by its fluorescence trajectory. As reported in the previous works [S1, S2], the CdSeTe/ZnS QDs used in the experiment have clearly distinguishable on- and off-state. On other word, the single QD will have a single on-state fluorescence intensity, as shown in Figure S5a. While the aggregated QDs or group of several QDs within the laser focusing area will emerge more than one on-state fluorescence intensity, due to the possible of synchronously photoemission from several QDs, as shown in Figure S5c.

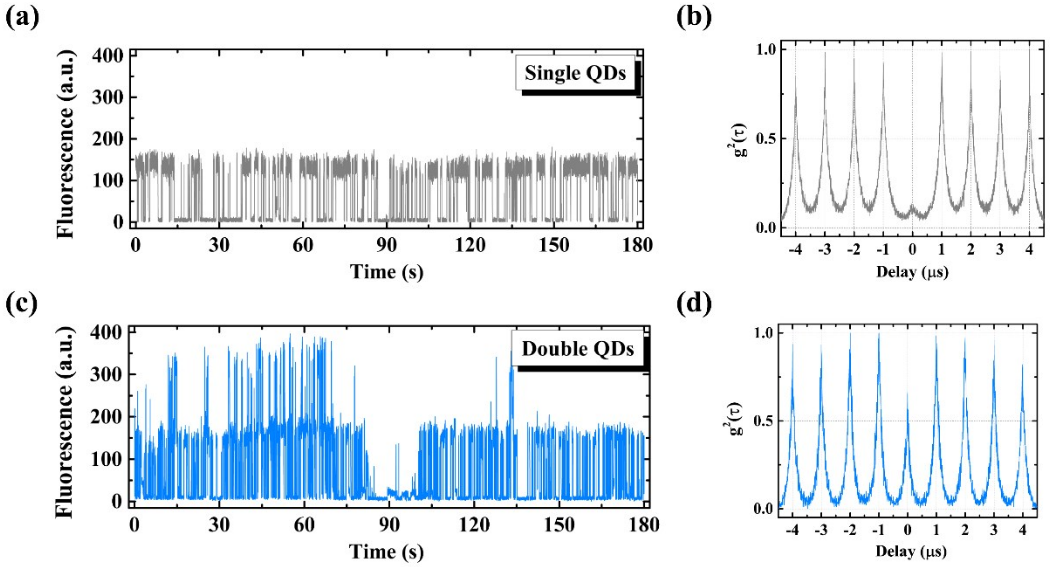

Figure S5. Fluorescence trajectories of single (a) and double QDs (b). Single QD shows a single on-state intensity, while double QDs show two on-state intensities, due to the two QDs may emit synchronously or alternately. (b) and (d) The $g^2(\tau)$ of the corresponding fluorescence emission.

Finally, the single QD will be further checked by its second-order correlation function, $g^2(\tau)$, which can characterize the probability of coincidence of two photons being detected with a time difference τ [S3]. QDs have now been demonstrated to be good single-photon source. Therefore, $g^2(\tau)$ for single QD will close to zero, while that for several QDs will be larger than 0.5, as shown in Figure S5b and S5d, respectively.

In our experiment, we checked the single QD by their fluorescence trajectories in most cases, and measured $g^2(\tau)$ as needed.

5. Lifetime measurements of QDs on glass, on PMMA and in toluene.

The purchased CdSeTe/ZnS QDs was dispersed in toluene. Before the manipulation of optical properties of QDs by laser irradiation, we have checked the photoemission properties of QDs in solution (toluene), on glass and on PMMA, they shared the similar fluorescence lifetime, as shown in Figure S6. Comparing with the lifetime changed by energy transfer and photoreduction, as presented in Figure 4, the slight difference between glass and PMMA can be ignored. Furthermore, the fluorescence intensity and photoblinking behavior of single QD on glass and on PMMA are similar, as well.

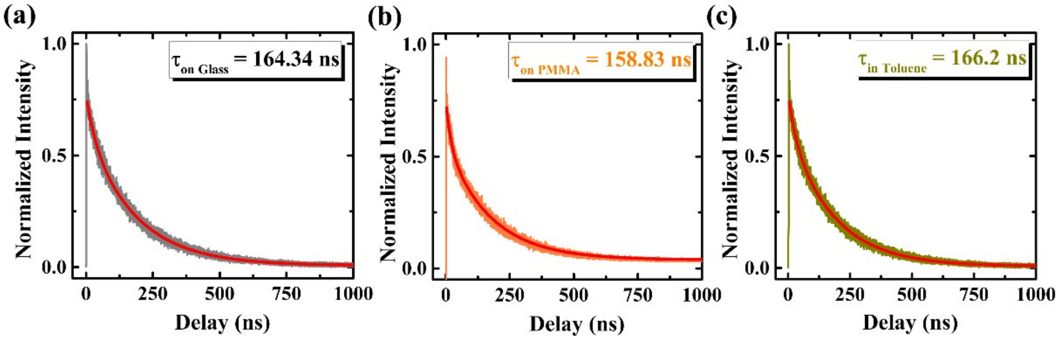

Figure S6. The time-resolved fluorescence decay and corresponding fitting results for ensemble QDs on glass (a), on PMMA (b), and in Toluene (c), respectively.

6. The stability of optical properties of QDs before and after CW laser irradiaion

According to the experimental results, the photoemission properties of QDs have no significantly change after strong laser irradiation, unless photobleaching. As shown in Figure S7, although there is a huge difference between the fluorescence intensities of QDs under pulse laser excitation and CW laser irradiation, the fluorescence intensities of QDs under pulse laser excitation before and after CW laser irradiation has no significant difference.

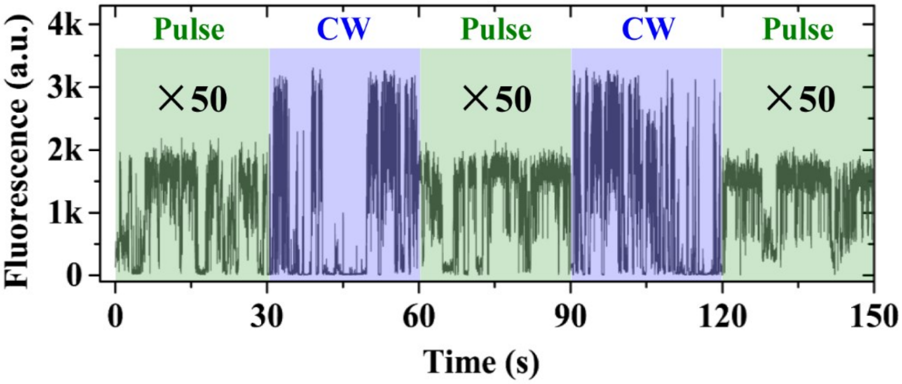

Figure S7. Fluorescence trajectory of single QD under pulse laser excitation and CW laser irradiation, respectively. The fluorescence intensity under pulse laser excitation has been enlarged by 50 times.

To further investigate the optical properties of QDs, we selected and compared the fluorescence trajectories before and after CW laser irradiation, as shown in Figure S8. It can be found that they emerges similar fluorescence intensity and blinking behaviors. The fluorescence lifetimes of two selected areas are also close, which are 148.6 ns and 145.9 ns, respectively.

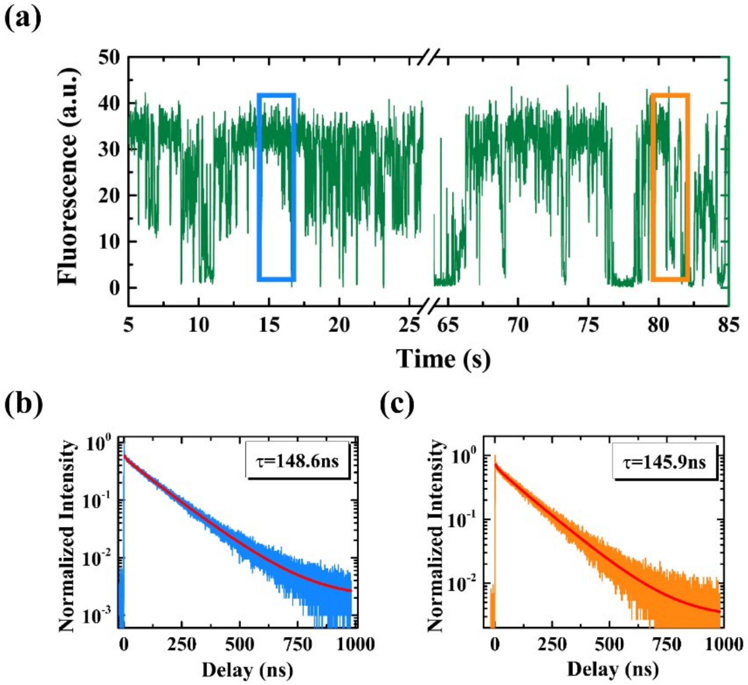

Figure S8. (a) Fluorescence trajectory of single QD under pulse laser excitation before and after CW laser irradiation. (b)-(c) The time-resolved fluorescence decay and fitting results of the selected areas (highlighted by rectangles).

7. Threshold fluorescence intensity for the separation of on- and off-state

The threshold fluorescence intensity, I_{th}, is defined to separate the on- and off-state,

$$I_{th} = I_{av} + 3\sigma \tag{S1}$$

where I_{av} is the average fluorescence intensity of the background, and σ is its standard deviation. Taking Figure S9 for individual QDs on glass as an example, the I_{av} is equal to 82 cps, σ is 16, yielding I_{th} to be 130 cps. According to this processing, the threshold fluorescence intensities for QDs on GO, RGO-1, 2, 3 are 476, 617, 401, 364 cps, respectively.

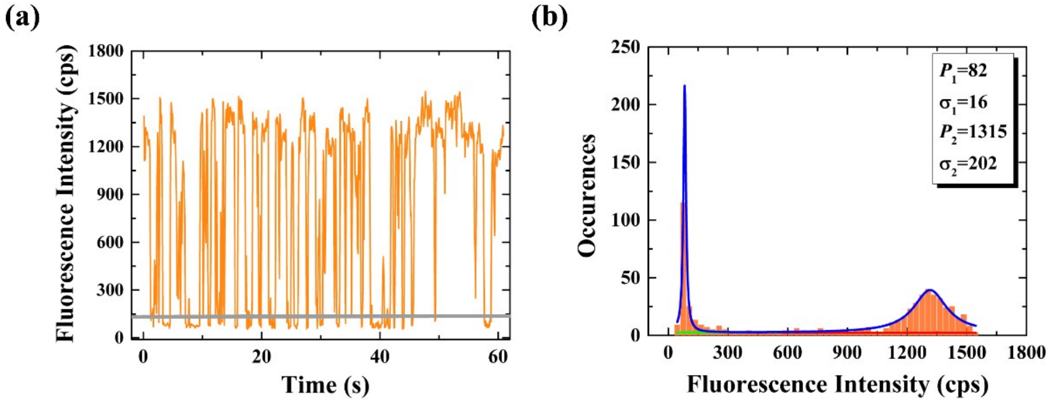

Figure S9. (a) Fluorescence trajectory and (b) photo counting histogram of CeSeTe/ZnS QDs on glass. The gray line in (a) represents the threshold separating on- and off-state, calculated according to equation S1.

8. Fluorescence trajectories, photo counts histograms and time-resolved fluorescence decays for QDs on RGO-1 and RGO-2

Detailed information about the fluorescence trajectories, photo counts histograms and time-resolved fluorescence decays for CdSeTe/ZnS QDs on RGO-1 and RGO-2 have been shown in Figure S10. The fluorescence intensities of QDs on RGO-1 and RGO-2 are 778 cps and 604 cps, respectively, while the lifetime for them are 117.5 ns and 83.6 ns, respectively. Thus, we can conclude that the interaction between QDs and RGO-1 and RGO-2 are stronger than that on GO, but weaker than that on RGO-3.

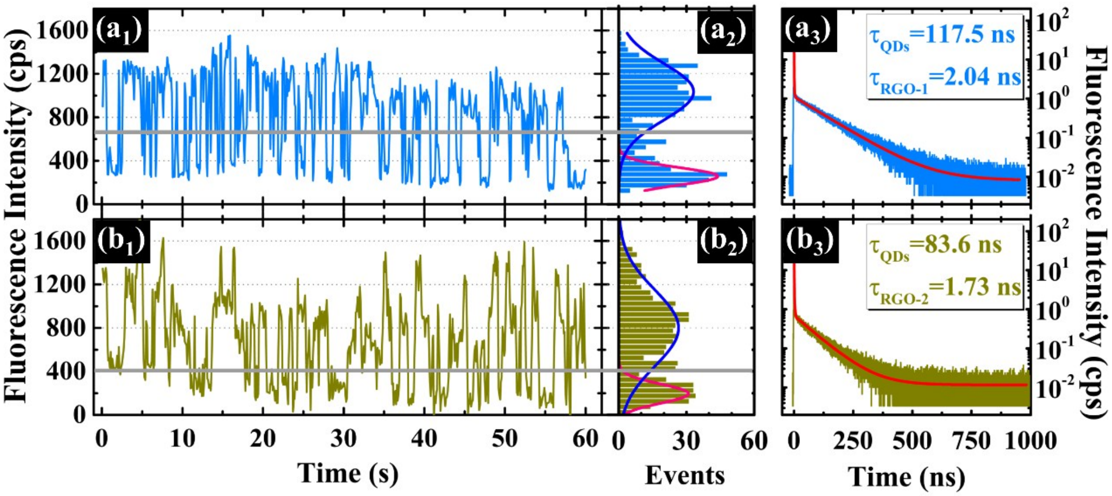

Figure S10. Fluorescence trajectories, photo counting histograms, and time-resolved fluorescence decays for individual CdSeTe/ZnS QDs on RGO-1 and RGO-2, respectively. The gray lines represent the thresholds separating on- and off-state.

9. Fluorescence histograms for QDs under different conditions

Similar to the lifetime histograms for CdSeTe/ZnS QDs on glass, GO and RGO-1, 2, 3, respectively, fluorescence histograms for QDs under these five conditions have been performed, as presented in Figure S11. All the fluorescence distributions can be fitted by Gauss function; the central values and the corresponding FWHM have been presented in Table S1.

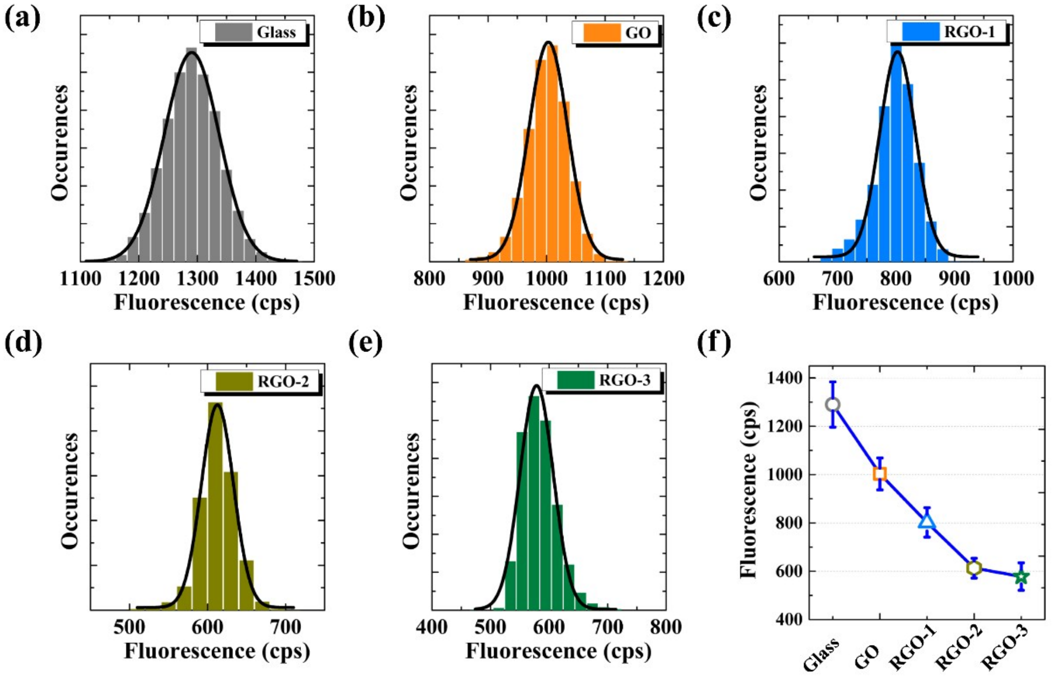

Figure S11. Fluorescence histograms for QDs on (a) glass, (b) GO, (c) RGO-1, (d) RGO-2, (e) RGO-3; (f) mean fluorescence for QDs under five conditions mentioned above, which were obtained from the Gauss fits of the histograms in panels a-e.

Table S1. The center values of fluorescence intensity and FWHM of QDs on glass, GO and RGO with different irradiation.

	Intensity (cps)	FWHM (cps)
Glass	1290	94
GO	1003	66
RGO-1	802	61
RGO-2	613	41
RGO-3	578	57

10. The influence of PMMA thickness to FRET

According to the classical Förster theory, the extent of energy transfer is determined by the distance between the donor (QDs) and acceptor (GO) [S4]. Thus, we inserted the transparent PMMA between QDs and GO to control the interaction strength at the stage of sample preparation, and then tune this interaction by photoreduction of GO as demand at the stage of practical applications.

To extend the tunability of energy transfer as large as possible, the thickness of PMMA has been optimized in the experiment. As shown in Figure S12b, when the thickness is 15 nm, the efficiency of energy transfer has been substantially changed from 24.4% to 65.4%. When the PMMA is too thin, the energy transfer between QDs and GO has been very strong. After photoreduction, the energy transfer cannot be substantially enhanced. As shown in Figure S12a, when the thickness of PMMA is 5 nm, after photoreduction, the efficiency of energy transfer only changes from 77.5% to 85.2%. On the other aspect, when the PMMA is too thick, even after photoreduction, the energy transfer between QDs and GO is still very weak. Thus, the energy transfer between QDs and RGO cannot be significantly improved, either. As shown in Figure S12c, when the thickness of PMMA is 34 nm, the efficiency of energy transfer only changes from 20.7% to 36.0%.

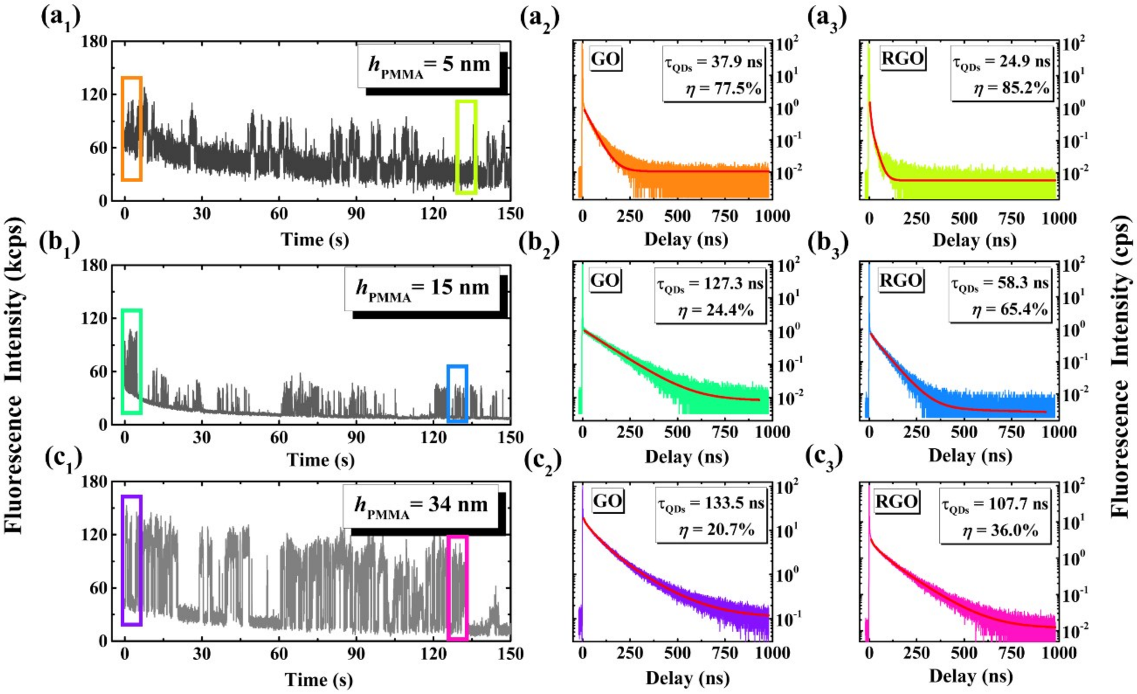

Figure S12. Fluorescence trajectories, time resolved fluorescence decays for individual QDs on GO and RGO with the thickness of PMMA films to be 5 nm, 15 nm, and 34 nm, respectively. The efficiencies (η) were determined by using $\tau_{QDs/Glass}$ of 168.4 ns (mean lifetime of statistical results).

---

11. References:

[S1]. Li, Z.; Zhang, G.; Li, B.; Chen, R.; Qin, C.; Gao, Y.; Xiao, L.; Jia, S., Enhanced biexciton emission from single quantum dots encased in N-type semiconductor nanoparticles. *Appl. Phys. Lett.*, 2017, **111** (15), 153106.

[S2]. Yang, C.; Zhang, G.; Feng, L.; Li, B.; Li, Z.; Chen, R.; Qin, C.; Gao, Y.; Xiao, L.; Jia, S., Suppressing the photobleaching and photoluminescence intermittency of single near-infrared CdSeTe/ZnS quantum dots with p-phenylenediamine. *Opt. Express*, 2018, **26** (9), 11889-11902.

[S3]. Enderlein, J.; Koberling, F.; Gryczynski, Z. K.; Kraemer, B.; Buschmann, V.; Erdmann, R.; Ruettinger, S.; Kapusta, P.; Patting, M.; Wahl, M.; Erdmann, R., Recent advances in photon coincidence measurements for photon antibunching and full correlation analysis. *Int. Soc. Opt. Photon.*, 2009, **7185**, 71850Q.

[S4]. Lakowicz, J. R., Energy Transfer. in *Principles of Fluorescence Spectroscopy*. Third Edition. New York : Kluwer Academic/Plenum, 1999; pp 13.